Rev. Roum. Sci. Techn.– Électrotechn. et Énerg.
Vol. **64**, *4*, pp. 397–402, Bucarest, 2019

THREE-PHASE FOUR-WIRE SHUNT ACTIVE FILTER BASED ON BACKSTEPPING CONTROLLER

ASMA BEN AMAR[1], LAID ZELLOUMA[1], MOHAMED TOUFIK BENCHOUIA[2], TIDJANI MAHNI[1]

Key words: Backstepping controller, Self-tuning filter, Synchronous reference frame, Three-phase four-wire shunt active filter, Total harmonic distortion (THD).

This paper deals with three-phase four-wire shunt active filter to improve power quality. It proposes backstepping control based on Lyapunov theory for the filter dc side voltage, and a modified synchronous reference frame approach based on two self-tuning filters for the identification of harmonic currents. The voltage source inverter of shunt active filter has a four-leg two-level topology. It is controlled by hysteresis. The proposed shunt active filter is verified by simulation and experimental validation. Backstepping control, an approach for nonlinear systems, leads to good dynamic and static performance in the dc side voltage control. Three-phase four-wire shunt active filter using the modified synchronous reference frame approach reduced the total harmonic distortion in the tested operating conditions.

1. INTRODUCTION

Starting with incandescent light bulbs, every load today creates harmonics. Electronic equipment like computers, battery chargers, electronic ballasts, variable frequency drives, and switching mode power supplies generates perilous amounts of harmonics. Issues related to harmonics are of greater concern to engineers and building designers because they do more than just distort voltage waveforms, they can overheat the building wiring, cause nuisance tripping, overheat transformer units, and cause random end-user equipment failures. As a result, active filters (AFs) have gained a lot of attention because of their excellent harmonic compensation [1].

Three-wire active filter provides compensation of harmonics and reactive power, but can't compensate zero sequence components caused by single-phase non-linear loads, inherently generates more harmonics than three-phase nonlinear loads. In fact, zero line may be overheated or causes a fire as a result of the excessive harmonic current [2]. For this reason, three-phase four-wire active filters (3P4WSAF) are recommended in distribution systems [3, 4].

The control of dc side voltage influences highly the performance of shunt active filter (SAF). Many works have dealt with 3P4W SAF as in [5–7]. Several control techniques and strategies have been developed in the literature as in [8–10]. Backstepping control based on Lyapunov theory is used to deal with the nonlinearity in SAF as in [11, 12].

This paper deals with 3P4W SAF to compensate harmonic currents. First, the system configuration is presented. Then, a modified synchronous referential frame (SRF) with self-tuning filters (STFs) is presented. After that, backstepping controller is developed to control dc side voltage. Finally, the simulation and experimental results with two nonlinear loads are presented and discussed.

2. SYSTEM CONFIGURATION

As it can be seen in Fig. 1, the power system is composed of 3P4W electrical source, that feeds two nonlinear loads through three inductors L_c. Nonlinear load-1 is composed of three single-phase diode bridge rectifiers, each rectifier is connected between phase and neutral and feeds a variable inductive load. Nonlinear load-2 is composed of: one single-phase diode bridge rectifier connected between phase ‘a’ and neutral to feed the inductive load, one single-phase diode bridge rectifier connected between phase ‘b’ and neutral to feed the inductive load, one single-phase dimmer connected between phase ‘c’ and neutral to feed a resistive load with $\alpha = 60^{\circ}$.

Three-phase four-wire SAF is composed of a four-leg two-level voltage source inverter (VSI) using insulated-gate bipolar transistor (IGBT) switches connected in parallel with a three-phase four-wire network through three inductors L_f. These inductors are used in order to minimize the noise injected by the VSI in the network. Four-leg VSI topology is preferred to be implemented as many researchers have appointed it as the most proficient alternative to be used in the SAF [5, 13]. The capacitor C_{dc} at the dc side of the VSI is used as dc energy source. In the experimental part, it is initially charged through the diodes of the VSI [14].

3. HARMONICS IDENTIFICATION

To identify harmonic currents of the three phases and the neutral from the side of the nonlinear load, SFR method used in [14] for three-wire networks is modified to be suitable for four-wire systems. The classical phase locked loop (PLL) is replaced by a PLL with STF.

As shown in Fig. 3 below, the load currents i_{la}, i_{lb} and i_{lc} are transformed into the αβo axis as follows:

$$\begin{bmatrix} i_\alpha \\ i_\beta \\ i_o \end{bmatrix} = \sqrt{\frac{2}{3}} \begin{bmatrix} 1 & -\frac{1}{2} & -\frac{1}{2} \\ 0 & \frac{\sqrt{3}}{2} & -\frac{\sqrt{3}}{2} \\ \frac{1}{\sqrt{2}} & \frac{1}{\sqrt{2}} & \frac{1}{\sqrt{2}} \end{bmatrix} \begin{bmatrix} i_{la} \\ i_{lb} \\ i_{lc} \end{bmatrix}. \quad (1)$$

As known, currents in the stationary frames can be respectively decomposed into fundamental and harmonic components by:

[1] University of El Oued, LEVRES Laboratory, Fac. Technology, 39000 El Oued, Algeria, E-mail: mahni-tidjani@univ-eloued.dz.
[2] University of Biskra, LGEB Laboratory, BP. 145, 07000, Biskra, Algeria.

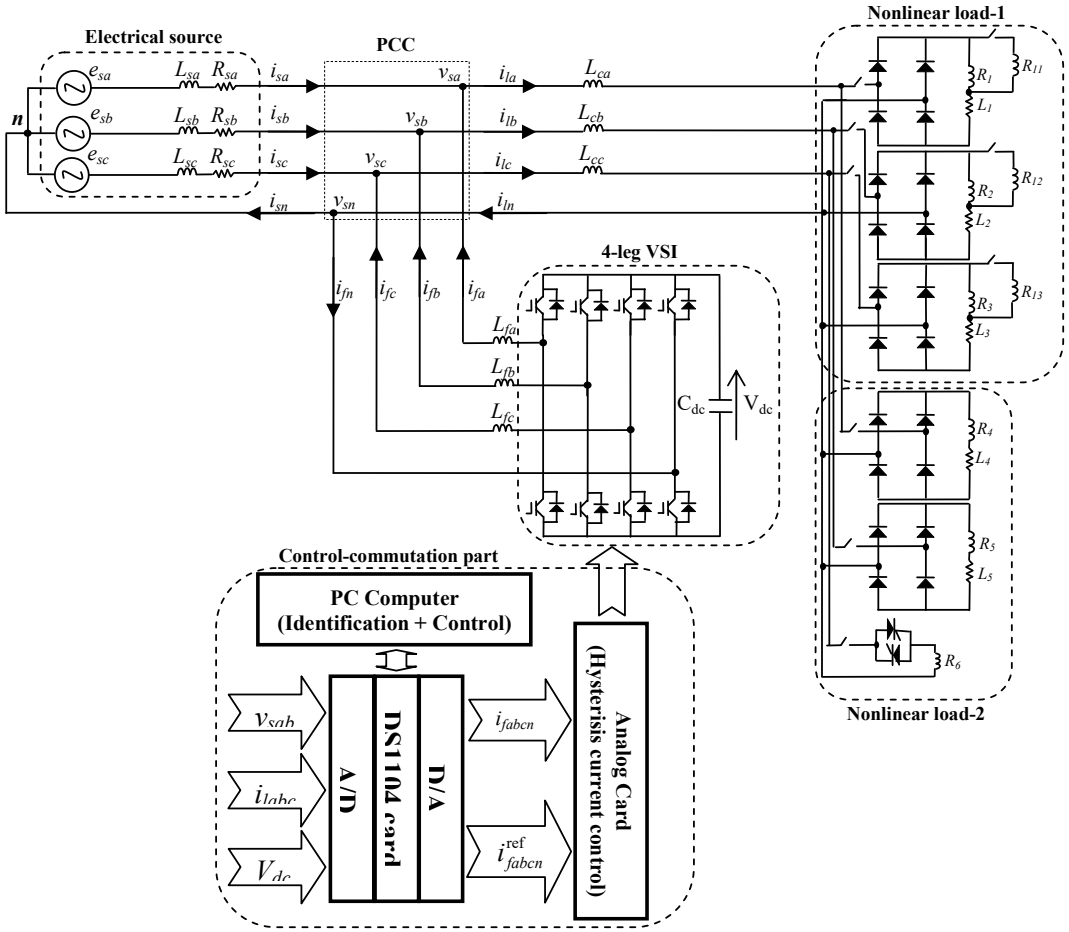

Fig. 1 – 3P4W SAF system configuration.

$$
\begin{aligned}
i_\alpha &= \bar{i}_\alpha + \tilde{i}_\alpha, \\
i_\beta &= \bar{i}_\beta + \tilde{i}_\beta, \\
i_o &= \bar{i}_o + \tilde{i}_o,
\end{aligned} \tag{2}
$$

$\bar{i}_\alpha, \bar{i}_\beta, \bar{i}_o$: fundamental components of the load currents.

$\tilde{i}_\alpha, \tilde{i}_\beta, \tilde{i}_o$: distortion components of the load currents.

Figure 2 shows the STF structure. This highly selective filter allows extracting the fundamental components at the pulsation ω_f directly from the distorted signal in the αβ axis. Its principle operation is based on the following equations:

$$
\bar{x}_\alpha = \frac{k}{s}\left[x_\alpha(s) - \bar{x}_\alpha(s)\right] - \frac{\omega_f}{s}\bar{x}_\beta(s), \tag{3}
$$

$$
\bar{x}_\beta = \frac{k}{s}\left[x_\beta(s) - \bar{x}_\beta(s)\right] - \frac{\omega_f}{s}\bar{x}_\alpha(s), \tag{4}
$$

x_α, x_β: input signals in the stationary frames,

$\bar{x}_\alpha, \bar{x}_\beta$: output signals (fundamental of the input signals),

ω_f: fundamental pulsation,

k: selectivity parameter (gain).

Then the αβ distortion currents components are computed by subtracting the STF input signals from the corresponding outputs. The resulting signals are $\tilde{i}_\alpha$ and $\tilde{i}_\beta$, which correspond to the distortion components of the load currents i_{la}, i_{lb} and i_{lc} in the stationary reference frame. The STF is used in the harmonic isolator instead of classical extraction filters (low pass (LPF) or high pass filters (HPF)).

The authors in [15] tested the selectivity of STF by varying the gain k. They observed that a small variation of this gain influences the filter selectivity. They also concluded that by decreasing k the selectivity of STF increases, but transient response time increases.

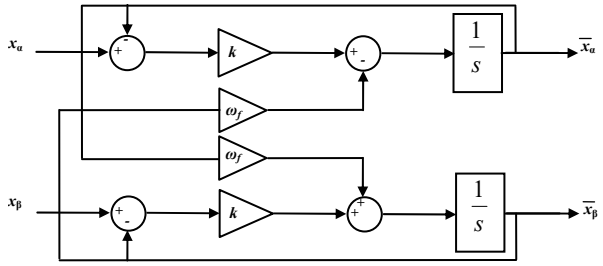

Fig. 2 – Self-tuning filter tuned to the fundamental pulsation.

The o component of the load current is composed of:

- $\tilde{i}_o$: harmonic current of order three and its odd multiple,
- $\bar{i}_o$: fundamental current (which is equal to zero in the case of balanced load).

Using the PLL with the proposed STF in [16] and mentioned in Fig. 3, $\cos(\theta)$ and $\sin(\theta)$ are generated from the source voltages v_{sa}, v_{sb} and v_{sc}.

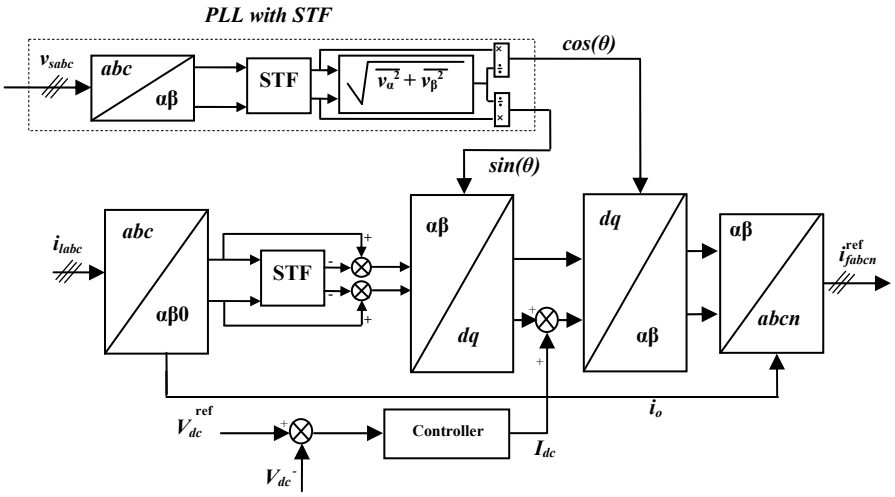

Fig. 3 – The modified SRF method for 3P4W SAF.

The currents expression in the *d-q* reference frame is given by:

$$\begin{bmatrix} \tilde{i}_d \\ \tilde{i}_q \end{bmatrix} = \begin{bmatrix} \sin(\theta) & -\cos(\theta) \\ \cos(\theta) & \sin(\theta) \end{bmatrix} \begin{bmatrix} \tilde{i}_\alpha \\ \tilde{i}_\beta \end{bmatrix}. \quad (5)$$

The reference currents expression in the αβ reference frame is given by:

$$\begin{bmatrix} i_\alpha^{ref} \\ i_\beta^{ref} \end{bmatrix} = \begin{bmatrix} \sin(\theta) & \cos(\theta) \\ -\cos(\theta) & \sin(\theta) \end{bmatrix} \begin{bmatrix} \tilde{i}_d + I_{dc} \\ \tilde{i}_q \end{bmatrix}. \quad (6)$$

I_{dc}: the output of voltage controller, which represents the necessary amount of active current to maintain dc side voltage constant.

Then the filter reference currents in *abcn* coordinates are defined by:

$$\begin{bmatrix} i_a^{ref} \\ i_b^{ref} \\ i_c^{ref} \\ i_n^{ref} \end{bmatrix} = \sqrt{\frac{2}{3}} \begin{bmatrix} 1 & 0 & \frac{1}{\sqrt{2}} \\ -\frac{1}{2} & \frac{\sqrt{3}}{2} & \frac{1}{\sqrt{2}} \\ -\frac{1}{2} & -\frac{\sqrt{3}}{2} & \frac{1}{\sqrt{2}} \\ 0 & 0 & \frac{3}{\sqrt{2}} \end{bmatrix} \begin{bmatrix} i_\alpha^{ref} \\ i_\beta^{ref} \\ i_o \end{bmatrix}. \quad (7)$$

In the experimental validation, these digital reference currents are the outputs of the DSPACE system. They are converted into analog signals by digital-to-analog converters. The measured currents i_{fabcn} are compared with i_{abc}^{ref}. Then, the switching patterns of the VSI are generated by an implemented (at LGEB laboratory) hysteresis current controller [14].

4. BACKSTEPPING CONTROLLER DESIGN

Classical proportional integral (PI) controller requires precise linear mathematical models, which are difficult to obtain. In addition, it can't give satisfactory performance under parameter variations and load disturbances. It causes a dc voltage overshoot and inrush reference currents which leads to protection or even equipment damage when SAF is plunged into the system. The voltage overshoot and the current inrush have been the constraints that restrict the development of SAF.

Backstepping control is based on Lyapunov theory. According to this theory a system is stable at the point x if there is a function continually derivable $U(x)$ that satisfies:

$$U(0) = 0, \quad (8)$$

$$U(0) > 0, \forall\ x \neq 0, x \in \Omega, \quad (9)$$

$$\dot{U}(0) < 0, \forall\ x \neq 0, x \in \Omega, \quad (10)$$

$\dot{U}(0)$: derivative of U at the point $x = 0$,

Ω: domain of study.

In order to control V_{dc} by the application of Lyapunov theory, let's consider the point $\Delta V_{dc} = V_{dc}^{ref} - V_{dc}$. This point should be near zero. The following expression is used:

$$E_{dc}(V_{dc}) = \frac{1}{2} C_{dc} V_{dc}^2, \quad (11)$$

E_{dc} : capacitor energy,

V_{dc} : dc side voltage,

V_{dc}^{ref} : dc side reference voltage.

For small variations of V_{dc}:

$$P_{dc}(V_{dc}) = \dot{E}_{dc}(V_{dc}) = C_{dc} V_{dc} \dot{V}_{dc} \Rightarrow \dot{V}_{dc} = \frac{P_{dc}(V_{dc})}{C_{dc} V_{dc}}. \quad (12)$$

The error is defined as:

$$\Delta E_{dc}(V_{dc}) = \frac{1}{2} C_{dc} \Delta V_{dc}^2. \quad (13)$$

To maintain this energy function stable, Lyapunov conditions must be satisfied. The first and the second conditions are satisfied. The derivative of ΔE_{dc} is given by:

$$\Delta \dot{E}_{dc}(V_{dc}) = \Delta P_{dc}(V_{dc}) < 0 \Rightarrow -C_{dc}\Delta V_{dc}\dot{V}_{dc} < 0 . \quad (14)$$

Substituting (12) in (14), the following expression is obtained:

$$-C_{dc}\Delta V_{dc}\frac{P_{dc}(V_{dc})}{C_{dc}V_{dc}} < 0 . \quad (15)$$

To satisfy the third condition, a constant $k > 0$ is introduced in such way that:

$$\frac{P_{dc}(V_{dc})}{V_{dc}} = \frac{\Delta V_{dc}}{k} , \quad (16)$$

so

$$P_{dc}(V_{dc}) = \frac{\Delta V_{dc}V_{dc}}{k} . \quad (17)$$

$P_{dc}(V_{dc})$ – the necessary active power to maintain V_{dc} constant.
By considering

$$P_{dc}(V_{dc}) = I_{dc}V_{dc}^{\text{ref}} , \quad (18)$$

the compensation current of V_{dc} is obtained as:

$$I_{dc} = \frac{P_{dc}(V_{dc})}{V_{dc}^{ref}} . \quad (19)$$

By choosing $k > 0$ the stability of dc side voltage is guaranteed, but the choice of the parameter k influences the performance of dc side voltage control. The optimal value of k is influenced by the 3P4W SAF system parameters. Simulations realized with MatLab/Simulink for the studied SAF confirm that:

- by increasing k the response time and the dynamical error ΔV_{dc} became very important,
- by decreasing k the response time and the dynamical error are reduced, but the static error became high.

In this work k = 1.44 is used, that gives better performance of backstepping controller.

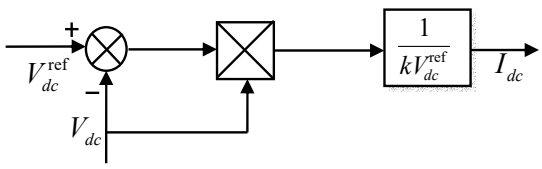

Fig. 4 – Backstepping controller.

5. SIMULATION AND EXPERIMENTAL RESULTS

According to the analysis above, SAF system is designed. The simulation is performed using MatLab/Simulink software. The parameters of 3P4W SAF system are shown in Table 3. The parameters of nonlinear loads are shown in Tables 1 and 2.

In the experimental test bench, the electric source is a step-down transformer (10.60 kVA), connected to the mains (380 V line to line). It delivers a line to neutral voltage of 110 V. The 3P4W SAF is achieved with a three-leg VSI and one leg of another VSI. Each VSI contains a three-leg IGBT 1200 V, 50 A (SKM 50 GB 123D). To ensure the dead time of control signals and the insulation, developed cards based on the IXDP630 component and a specialized circuit (SKHI 22) is used. Analog card is used to generate current hysteresis control of IGBTs. The experimental test bench is built around the DSPACE-1104. The values of V_{sabc}, I_{labc} and V_{dc} are obtained by sensors. They are used in the identification process. The value of i_{fabcn}^{ref} is converted into analog to be used in the analog hysteresis card. The used probes by currents and voltages sensors are respectively 10× and 200×.

The simulation and experimental results for each case are given in the figures below.

Figures 5 and 6 show the simulation and experimental results under unbalanced nonlinear load-1. Before the insertion of SAF, the source currents are distorted. The THDs of the source currents are 20.43 %, 32.12 %, 21.21 % for phases ‘a’, ‘b’ and ‘c’ respectively. After the insertion of the SAF, the source currents became perfectly sinusoidal. The THDs of the source currents are reduced to 4.09 % for phase ‘a’, 4.43 % for phase ‘b’ and 4.17 % for phase ‘c’ which are below the recommended limit (5 %), while the neutral current is canceled.

Figures 7 and 8 show the simulation and experimental results during the change of loads. These results show that response time is very small and the source currents stay sinusoidal. While experimental results show that currents magnitudes are greater than currents magnitudes obtained by simulation. A small currents distortion can be noticed in experimental result.

Figures 9 and 10 show the simulation and experimental results under unbalanced nonlinear load-2. Before the insertion of SAF, the source currents are distorted. The THDs of phases a, b and c are respectively 12.37 %, 30.91 % and 30.37 %. After the SAF insertion, the source currents became sinusoidal and the neutral current became zero. The THDs of the source currents are reduced to 4.18 % for phase a, 4.37 % for phase b and 4.79 % for phase c.

Figures 11 and 12 show the identification currents obtained by simulation and experimentation.

To prove the dynamical performance of backstepping controller, the dc side resistances are changed from R_1, R_2 and R_3 to R_{11}, R_{12} and R_{13} at 0.4 s. It is clear from simulation results (Fig. 13) that a good transient performance of the source current is obtained. Dc side voltage follows its reference (350 V) and the source current maintains its sinusoidal waveform. Figure 14 shows the corresponding experimental results.

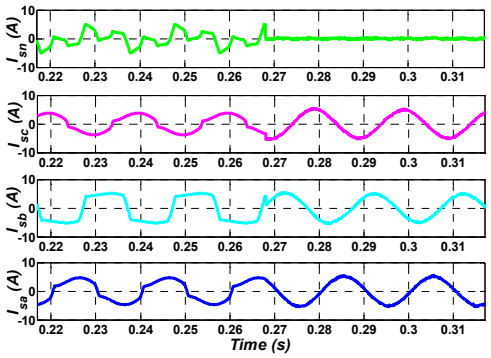

Fig. 5 – Simulation - SAF insertion (nonlinear load 1).

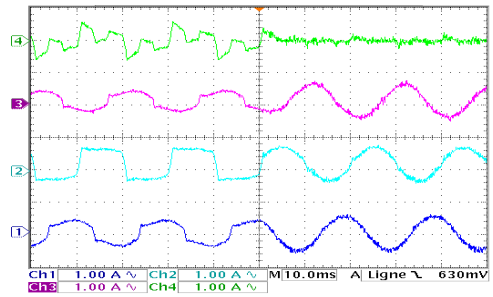

Fig. 6 – Experimental - SAF insertion (nonlinear load 1). i_{sa}, i_{sb}, i_{sc}, and i_{sn} (Ch1, Ch2, Ch3, and Ch4): 10 A/div, Time scale: 0.1 s/div.

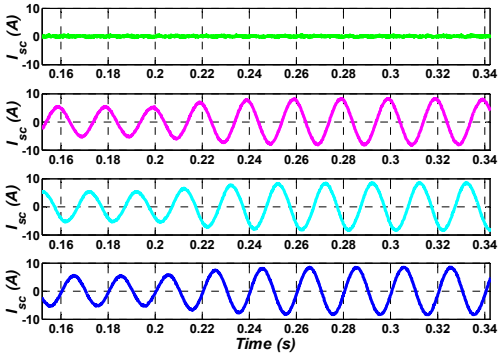

Fig. 7 – Simulation - Load variation (nonlinear load 1).

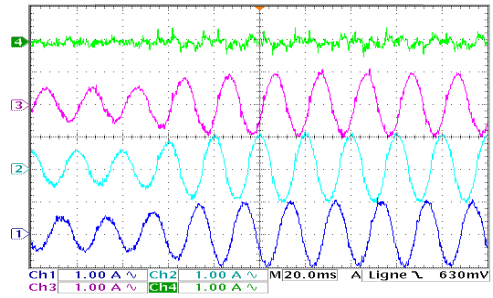

Fig. 8 – Experimental - Load variation (nonlinear load 1). i_{sa}, i_{sb}, i_{sc}, and i_{sn} (Ch1, Ch2, Ch3, and Ch4): 10 A/div, Time scale: 0.1 s/div.

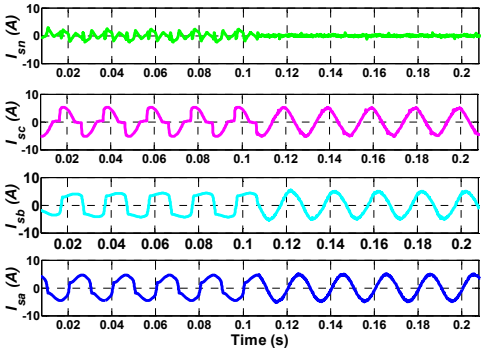

Fig. 9 – Simulation - SAF insertion (nonlinear load 2).

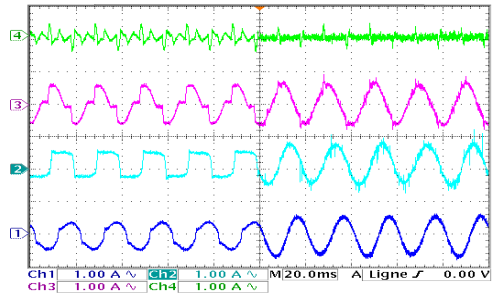

Fig. 10 – Experimental - SAF insertion (nonlinear load 2). i_{sa}, i_{sb}, i_{sc}, and i_{sn} (Ch1, Ch2, Ch3, and Ch4): 10 A/div, Time scale: 0.1 s/div.

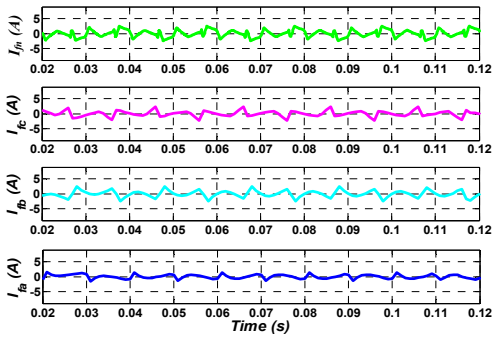

Fig. 11 – Simulation - SAF currents (nonlinear load 2).

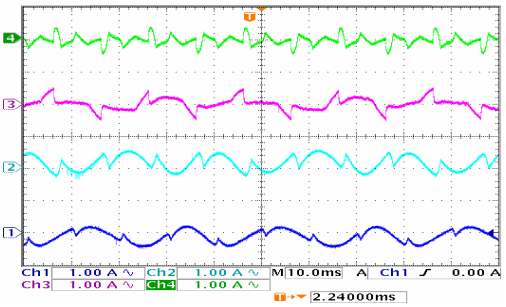

Fig. 12 – Experimental - SAF currents (nonlinear load-2). i_{fa}, i_{fb}, i_{fc}, and i_{fn} (Ch1, Ch2, Ch3, and Ch4): 10 A/div, Time scale: 0.1 s/div.

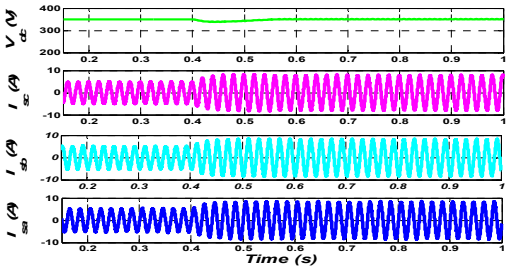

Fig. 13 – Simulation - Load variation (nonlinear load-1).

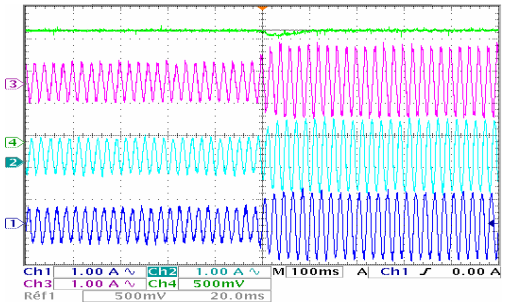

Fig. 14 – Experimental - Load variation (nonlinear load-2). i_{sa}, i_{sb} and i_{sc} (Ch1, Ch2 and Ch3): 10 A/div, V_{dc} (Ch4) 100 V/div, Time scale: 0.1 s/div.

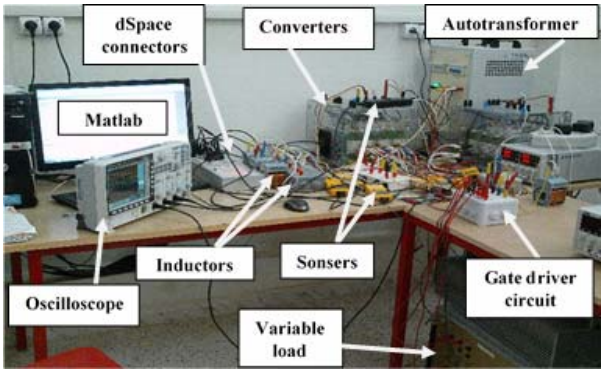

Fig.15 – The photograph of the experimental test bench.

6. **CONCLUSION**

In this paper, backstepping controlled 3P4W SAF with the modified SRF method is simulated and implemented in order to improve the performance of harmonic currents mitigation.

The simulation and experimental results demonstrate that the proposed SAF leads to good performances in both dynamic and steady state conditions. Backstepping controller gives a rapid response, low voltage undershoot in dynamic regime. It doesn't make any overshoot. In addition, backstepping controller permits to avoid precise mathematical models required by PI controller. The modified SRF with STF proved the ability to identify harmonics. The THD is well below the limit of 5 % imposed by the IEEE 519-2014.

Received on June 18, 2018

APPENDIX

Table 1

Nonlinear load 1 parameters

	Phase a	**Phase b**	**Phase c**
Resistance (Ω)	$R_1 = 20$ $R_{11} = 23.5$	$R_2 = 12.4$ $R_{12} = 6.6$	$R_3 = 28$ $R_{13} = 21.3$
Inductance (mH)	$L_1 = 21.1$	$L_2 = 200$	$L_3 = 21.1$

Table 2

Nonlinear load-2 parameters

	Phase a	**Phase b**	**Phase c**
Resistance (Ω)	$R_4 = 20$	$R_5 = 16.5$	$R_6 = 18.6$
Inductance (mH)	$L_4 = 33$	$L_5 = 200$	$L_6 = 0$

Table 3

Power system parameters

Supply	Voltage	V_S	110 V
	Frequency	f	50 Hz
	Resistance	R_s	0.42 Ω
	Inductance	L_s	2.3 mH
Filter	Dc capacitor	C_{dc}	1100 µF
	Dc voltage	V_{dc}	350 V
	Inductance	L_f	3 mH
	Hysteresis band	Δi	0.02 A
ac side	Inductance	L_c	1 mH
STF	Selectivity parameter	k	60

REFERENCES

1. S. Mikkili, A. K. Panda, *PI and fuzzy logic controller based 3-phase 4-wire shunt active filters for the mitigation of harmonic currents with the Id-Iq control strategy*, Journal of power electronics, **11**, *6*, pp. 914–921 (2011).
2. S. Mikkili, A.K. Panda, *PI and Fuzzy Controller based SHAF for Mitigation of Current Harmonics with Id-Iq Control Strategy*, Journal of Electrical Engineering, **12**, *2*, (2012).
3. F. Hamoudi, A. Chaghi, M. Adli, H. Amimeur, *A sliding mode control for four-wire shunt active filter*, Journal of Electrical Engineering, **62**, 5, pp. 267–273 (2011).
4. M. Ucar, E. Ozdemir, *Control of a 3-phase 4-leg active power filter under non ideal mains voltage condition*, Electric Power Systems Research, **78**, *1*, pp. 58–73 (2008).
5. T. Mahni, M.T Benchouia, K. Srairi, A.Ghamri, A.Golea , *Three-phase four-wire shunt active filter with unbalanced loads,* Energy procedia, **50**, pp. 528–535 (2014).
6. M.C. Benhabib, S. Saadate, *New control approach for four-wire active power filter based on the use of synchronous reference frame*, Electric Power Systems Research, **73**, pp. 353–362 (2004).
7. A. Chebabhi, M. Fellah, A. Kessal, M. Benkhoris, *Comparative study of reference currents and dc bus voltage control for Three-Phase Four-Wire Four-Leg SAF to compensate harmonics and reactive power with 3D SVM*, ISA Transactions, **57**, pp. 360–372 (2015).
8. S. Chennai, *Three-level neutral point clamped shunt active power filter performances using intelligent controllers*, Rev. Roum. Sci. Tech-électrotechn. et Energ., **59**, *3*, pp. 303–313 (2016).
9. L. Deng, J. Fei, C. Cai, Global fast terminal sliding mode control for an active power filter based on a backstepping design, Rev. Roum. Sci. Tech-électrotechn. et Energ., **61**, *3*, pp. 293–298 (2016).
10. A. Chebabhi, M.K. Fellah, M.F. Benkhoris, *3D space vector modulation control of four-leg shunt active power filter using pqo theory*, Rev. roum. Sci. Tech-électrotechn. et Energ., **60**, 2, pp. 185–194 (2015).
11. Y. Fang, S. Hou, J. Fei, *Harmonic suppression of three-phase active power filter using backstepping approach*, International Journal of Innovative Computing, Information and Control, **11**, *2*, pp. 419–507 (2015).
12. M. Bouzidi, S. Bouafia, A. Benaissa, A. Bouzidi, S. Barkat, *Backstepping control of three-phase four-leg shunt active power filter*, Journal of Electrical Engineering, **14**, *3*, pp. 358–363 (2014).
13. L. Zellouma, B. Rabhi, A. Karma, A. Benaissa, M.F. Benkhoris, *Simulation and real time implementation of three phase four wire shunt active power filter based on sliding mode controller*, Rev. roum. Sci. Tech-électrotechn. et Energ., **63**, *1*, pp. 77–82 (2014).
14. M.T. Benchouia, I. Ghadbane, A. Golea, K. Srairi, M.E.H. Benbouzid, *Implementation of adaptive fuzzy logic and PI controllers to regulate the dc bus voltage of shunt active power filter*, Applied soft computing, **28**, pp. 125–131 (2015).
15. M. Abdusalam, P. Pourbe, S. Karimi, S. Saadate, *New digital reference current generation for shunt active power filter under distorted voltage conditions*, Electric Power Systems Research, **79**, pp. 759–765 (2009).
16. A. Boussaid, A. L. Nemmour, L. Louze, A. Khezzar, *A novel strategy for shunt active filter control*, Electric Power Systems Research, **123**, pp. 154–163 (2015).